Collision strengths for FIR and UV transitions in P III and the phosphorus abundance

Rahla Naghma,[1]★ Sultana N. Nahar[1]★ and Anil K. Pradhan[1,2,3]★

[1]*Department of Astronomy, The Ohio State University, Columbus, OH 43210, USA*
[2]*Chemical Physics Program, The Ohio State University, Columbus, OH 43210, USA*
[3]*Biophysics Graduate Program, The Ohio State University, Columbus, OH 43210, USA*

ABSTRACT

Phosphorus abundance is crucial for DNA-based extraterrestrial life in exoplanets. Atomic data for observed spectral lines of P-ions are needed for its accurate determination. We present the first calculations for collision strengths for the forbidden [P III] fine structure transition $3s^2 3p(^2P^o_{1/2-3/2})$ within the ground state at 17.9 µm, as well as allowed UV transitions in the $3s^2 3p(^2P^o_{1/2,3/2}) \rightarrow 3s3p^2(^2D_{3/2,5/2}, {}^2S_{1/2}, {}^2P_{1/2,3/2})$ multiplets between 915 and 1345 Å. Collision strengths are computed using the Breit–Pauli R-Matrix method including the first 18 levels, and they exhibit extensive auto-ionizing resonance structures. In particular, the Maxwellian averaged effective collision strength for the FIR 17.9 µm transition shows a factor 3 temperature variation broadly peaking at typical nebular temperatures. Its theoretical emissivity with solar phosphorus abundance is computed relative to H β and found to be similar to observed intensities from planetary nebulae; the abundances derived in earlier works are 3–5 times sub-solar. The results pertain to the reported paucity of phosphorus from preferred production sites in supernovae, and abundances in planetary nebulae and supernova remnants.

Key words: astrobiology – atomic processes – ISM: atoms – ISM: supernova remnants – ISM: nebulae; infrared: general.

1 INTRODUCTION

Phosphorus abundance is of considerable interest in the search for life forms in exoplanets. It is the backbone element in the DNA molecule, enabling chemical bonds among myriad nucleotides that constitute the complex double-helical structure. However, ascertaining nucleosynthesis pathways and determining the actual abundance of phosphorus ($Z = 15$) is challenging because it is much lower than low-Z α-elements, and orders of magnitude lower than the other five most common elements of the six that constitute the CHONPS-based life organisms on the Earth. The photospheric solar abundances numerically relative to hydrogen are (Asplund et al. 2009): C (2.7×10^{-4}), N (6.8×10^{-5}) O (4.9×10^{-4}), P (2.6×10^{-7}), and S (1.3×10^{-5}).

Phosphorus abundances have been measured from the mid-infrared [P III] 17.9 µm observations of late stages of stellar remnants such as planetary nebulae (Pottasch & Bernard-Salas 2008; Pottasch, Bernard-Salas & Roelig 2008; Otsuka et al. 2011) and from ground-based observations of F,G,K dwarf stars (Maas, Pilachowski & Cescutti 2017). Whereas phosphorus, with an odd

atomic number $Z = 15$, can be synthesized during the asymptotic giant branch phase of low-mass stars, it is thought to be mainly produced in evolutionary stages of massive stars, before and during supernovae explosion by neutron capture with silicon. An analysis using singly ionized P II lines found up to 100 times the P/Fe ratio in the young core-collapse SNR Cassiopeia A than the Milky Way average (Koo et al. 2013). Phosphorus is chemically very reactive, so its low gas phase abundance may also be difficult to determine due to dust and grain formation.

Despite its astrophysical and increasing astrobiological importance, theoretical spectral analysis is hampered by the paucity of radiative and collisional atomic data for phosphorus ions. It is surprising that very little data for the important low-ionization stages of P-ions in stellar and nebular sources are available, relative to nearly all other first- and second-row elements (viz. Pradhan & Nahar 2011). Electron impact excitation cross-sections for P I have been calculated in the Born approximation for excitations from the ground 3p up to several $n\ell$ sub-orbitals (Ganas 1998). Elaborate Dirac R-Matrix calculations for photoionization of low-lying ground and metastable levels of P III have been done over a small photon energy range, with good agreement with experimental measurements (Wang, Jiang & Duan 2016). Recently, sophisticated Breit–Pauli R-Matrix (BPRM) calculations have been carried out for photoionization of a large number of P II levels using an 18-level

★ E-mail: pradhan.1@osu.edu (AKP); rahlanaghma@gmail.com (RN); nahar.1@osu.edu (SNN)

coupled channel wavefunction expansion for P III (Nahar 2017a,b; Nahar et al. 2017); very good agreement was found with the experimental P II photoionization cross-sections measured at the Berkeley *Advanced Light Source*, particularly for the detailed resonance structures in the near-threshold region. These earlier works form the basis for the calculations reported in this letter.

There are no other previous calculations for collisional excitation of low-ionization stages of P-ions. We also develop an atomic physics framework for astrophysical spectral diagnostics in nebular environments as function of temperature, density, and ionization equilibrium, potentially leading to more accurate abundance determination.

2 PHOSPHORUS ABUNDANCE ANALYSIS

Previous works are based on observational analysis of relative intensities of phosphorus lines compared to other elements. For example, nebular abundances have been determined in planetary nebulae (PNe) NGC 3242 and NGC 6369 from mid-IR observations of [P III] forbidden 17.9 μm line using the *Infrared Spectrograph* aboard the *Spitzer Space Telescope* and the *Short Wavelength Spectrograph* on the *Infrared Space Observatory* (Pottasch & Bernard-Salas 2008) and NGC 2392 (Pottasch, Bernard-Salas & Roelig 2008). A comparison of abundances for NGC 3242 shows phosphorus underabundance in a number of PNe, by a factor of 5 relative to solar, and more than a factor of 3 in NGC 6369. The large discrepancies are attributed to dust formation (Pottasch & Bernard-Salas 2008). However, the results are model dependent since they entail atomic parameters and ionization fractions not known to high precision.

For a single observed line the ion abundance may be derived from the measured intensity ratio under certain conditions. Relative to recombination line H β, we may write (Pottasch & Beintema 1999)

$$\frac{I_{\text{ion}}}{I_{\text{H}\beta}} = N_e \frac{N_{\text{ion}}}{N_{p+}} \frac{\lambda_{\text{H}\beta}}{\lambda_{ji}} \frac{A_{ji}}{\alpha_R(\text{H}\beta)} \left(\frac{N_j}{N_{\text{ion}}}\right), \quad (1)$$

where N_{ion} is the ionic abundance, N_j is the upper level population, A_{ji} is the Einstein decay rate between levels $j \rightarrow i$, and α_R is the H β-recombination coefficient. The present case of [P III] is similar to the well-known C II 157 μm line emitted via the $2s^2 2p^2 P^o_{1/2-3/2}$ transition (Blum & Pradhan 1991). Theoretically, we write line emissivity for the [P III] FIR transition formed with a given phosphorus abundance as (Pradhan & Nahar 2011)

$$\epsilon(17.9\,\mu\text{m}) = \frac{h\nu A(^2P^o_{3/2} - {}^2P^o_{1/2})}{4\pi} \times \frac{N(^2P^o_{3/2})}{\sum_i N_i(\text{P\,III})} \times \frac{n(\text{P\,III})}{n(\text{P})}$$
$$\times \frac{n(\text{P})}{n(\text{H})} \times n(\text{H})\ \text{ergs cm}^{-3}\,\text{s}^{-1}. \quad (2)$$

The sum in the denominator on the right-hand side of equation (2) refers to all levels included in the atomic model. Calculating the level populations requires rate coefficients for contributing atomic processes that may be due to recombination cascades, electron impact excitation, and fluorescent excitation from an external radiation field. In addition, equation (2) also depends on ionization balance for existing states in the plasma, as well as the elemental abundance itself – the quantity to be determined. However, if the two closely spaced levels are effectively decoupled from other levels in the ion then a simple expression gives the emissivity in terms of only the electron impact excitation rate coefficient and transition energy $h\nu$,

$$\epsilon(^2P^o_{3/2} - {}^2P^o_{1/2}) = N_e N_{\text{ion}} q(^2P^o_{3/2} - {}^2P^o_{1/2}) h\nu/4\pi. \quad (3)$$

Equation (3) implicitly assumes that all excitations to the upper level $^2P^o_{3/2}$ would be followed by downward decay to the ground state $^2P^o_{1/2}$, leaving the temperature-dependent electron impact excitation rate coefficient q as the only important quantity to be calculated. That, in turn, is related to the Maxwellian averaged effective collision strength $\Upsilon_{ij}(T_e)$ as

$$q_{ij}(T_e) = \frac{g_j}{g_i} q_{ji} e^{-E_{ij}/kT_e} = \frac{8.63 \times 10^{-6}}{g_i T^{1/2}} \Upsilon(T_e), \quad (4)$$

and

$$\Upsilon_{ij}(T_e) = \int_0^\infty \Omega_{ij}(E) \exp(-E/kT_e) \text{d}(E/kT_e), \quad (5)$$

where E_{ij} is the energy difference and Ω_{ij} is the collision strength for the transition $i \rightarrow j$. The exponentially decaying Maxwellian factor implies that at low temperatures only the very low energy $\Omega_{ij}(E))$ would determine the $\Upsilon(T_e)$. Furthermore, the detailed $\Omega(E)$ is generally a highly energy-dependent function due to autoionizing resonances, which leads to temperature sensitivity in the rate coefficient $q(T_e)$ via $\Upsilon(T_e)$ as in equations (4) and (5).

3 THEORY AND COMPUTATIONS

A brief theoretical description of the calculations is given. In particular, we describe relativistic effects and the representation of the (e + ion) system.

3.1 Relativistic fine structure

The relativistic Hamiltonian (Rydberg units) in the BPRM approximation is given by

$$H_{N+1}^{\text{BP}} = \sum_{i=1}^{N+1} \left\{ -\nabla_i^2 - \frac{2Z}{r_i} + \sum_{j>i}^{N+1} \frac{2}{r_{ij}} \right\} + H_{N+1}^{\text{mass}} + H_{N+1}^{\text{Dar}} + H_{N+1}^{\text{so}}, \quad (6)$$

where the last three terms are one-body relativistic corrections of the Breit interaction, respectively:

the mass correction term, $H^{\text{mass}} = -\frac{\alpha^2}{4} \sum_i p_i^4$,
the Darwin term, $H^{\text{Dar}} = \frac{Z\alpha^2}{4} \sum_i \nabla^2(\frac{1}{r_i})$, $\quad$ (7)
the spin-orbit interaction term, $H^{\text{so}} = Z\alpha^2 \sum_i \frac{1}{r_i^3} \mathbf{l_i} . \mathbf{s_i}$.

3.2 Wavefunction representation and calculations

Based on the coupled channel approximation, the R-matrix method (Burke 2011) entails a wavefunction expansion of the (e + ion) system in terms of the eigenfunctions for the target ion. In the present case we are interested in low-lying FIR transition within the ground configuration $3s^2 3p$ and the next excited configuration $3s3p^2$. Therefore we confine ourselves to an accurate wavefunction representation for the first 18 levels dominated by the *spectroscopic* configurations $[1s^2, 2s^2, 2p^6]3s^2 3p(^2P^o_{1/2,3/2})$, $3s3p^2(^4P_{1/2,3/2,5/2}, {}^2D_{3/2,5/2}, {}^2S_{1/2}, {}^2P_{1/2,3/2})$, $3s^2 3d(^2D_{3/2,5/2})$, $3s^2 4s(^2S_{1/2})$, $3s^2 4p(^2P^o_{1/2,3/2})$, $3p^3(^4S^o_{3/2}, {}^2D^o_{3/2,5/2}, {}^2P^o_{1/2,3/2})$. The atomic structure calculations using the code SUPERSTRUCTURE (Eissner et al. 1974) and the BPRM calculations are described in Nahar (2017a). The calculated and experimentally observed energies generally agree to within 5 per cent for all levels; the relatively small and sensitive fine structure splitting differs by 15 per cent (Nahar 2017a).

Fig. 1 presents the Grotrian energy level diagram of P III. As noted above, the ground state $3s^2 3p\,^2P^o_{1/2,3/2}$ fine structure is well
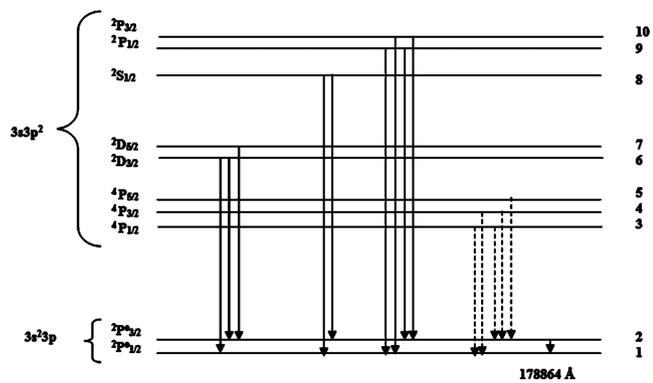
Figure 1. Energy diagram of P III showing the ground $3s^2 3p$ and the first excited configuration $3s 3p^2$ levels. The energy separation of the ground state fine structure $^2P^o_{1/2,3/2}$ transition at 17.9 μm is 0.0051 Ry, and well separated from the dipole allowed UV transitions of the $^2P^o_{1/2,3/2}$–$^2D, ^2S, ^2P$ multiplets between 915 and 1345 Å with $E > 0.68$ Ry.

separated by about 0.6 Ry or 7 eV from the next excited $3s 3p^2$ configuration terms and levels (Nahar 2017a; see Pradhan & Nahar 2011 for a general description of atomic processes and calculations). By comparison, in C II it is less than 0.4 Ry, and approximation in equation (4) has been utilized assuming that the Boltzmann factor $\exp(-E_{ij}/kT)$ effectively decouples the electron impact excitation of the forbidden FIR transition from higher levels of the ion (equation 4). For example, at $T_e = 10^4$ K we have $\exp(-E/kT) \approx \exp(-16E)$ and the value of $q(T_e)$ for allowed UV transitions is orders of magnitude lower compared to the FIR transition. Even though the observed and experimental values are close, a small difference in resonance positions relative to threshold can introduce a significant uncertainty in the effective collision strengths. The observed energies were substituted for theoretical ones in order to reproduce the threshold energies more accurately. This is of particular importance for excitation at low temperatures dominated by near-threshold resonances.

The BPRM collision strengths were computed up to 5 times the energy of the highest level in the atomic calculations, $3p^3(^4S^o_{3/2})$ at 1.45 Ry. Particular care is taken to test and ensure convergence of collision strengths with respect to partial waves and energy resolution. Total (e + ion) symmetries up to $(LS)J\pi$ with $J \leqslant 19.5$ were included in the calculations, though it was found that the collision strengths for forbidden transitions converged for $J \leqslant 7$. An energy mesh of $\Delta E \sim 10^{-5}$ Ry was used to resolve the near-threshold resonances. The resonances were delineated in detail prior to averaging over the Maxwellian distribution.

4 RESULTS

We describe the two main sets of results for the FIR and the UV transitions, as well as the diagnostic lines. Collision strengths have been computed for all 153 transitions among the 18 P III levels. Selected results are presented below; no previous data are available for comparison.

### 4.1 The forbidden 17.9 μm transition

The calculated fine structure collision strength is shown in Fig. 2(a), which exhibits considerable autoionizing resonance structures and energy dependence throughout the range up to the highest level of the P III ion included in the BPRM wavefunction expansion,
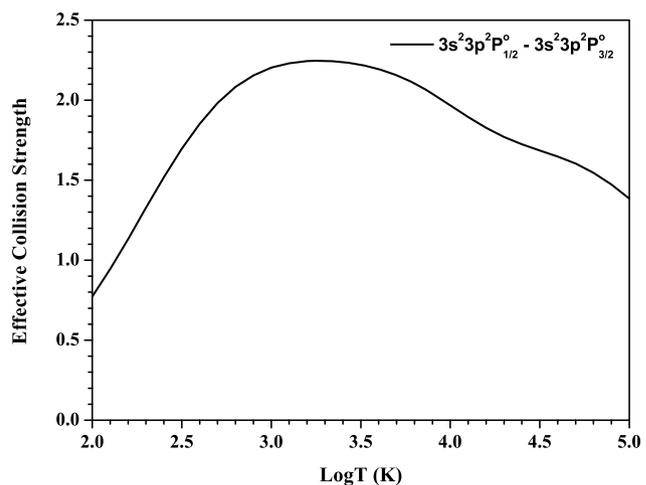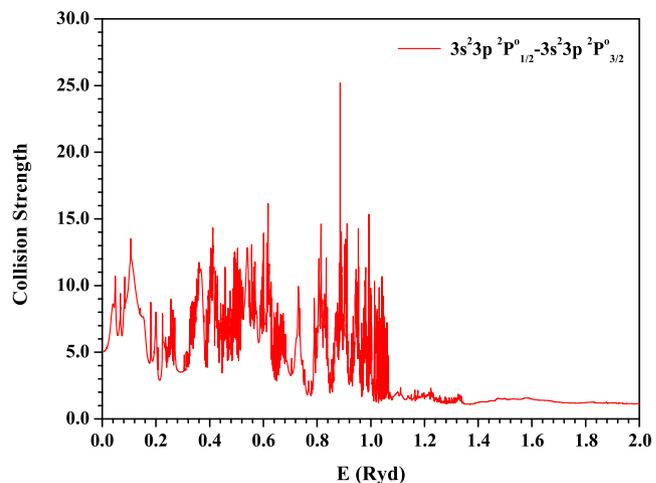
Figure 2. (a) Collision strength for the 17.9 μm [P III] IR fine structure transition. High resolution at near-threshold energies is necessary for accuracy in rate coefficients at low temperatures. (b) Maxwellian averaged effective collision strengths $\Upsilon(T_e)$ (equation 5). There is a factor of 3 or more variation broadly peaking at typical nebular temperatures $T_e > 10^3$ K. structures.

$E(3p^3 \ ^2P^o_{3/2}) = 1.45$ Ry. The fall-off for $E > 1.0$ Ry indicates that the collision strength is much lower at higher energies, and has converged for this forbidden transition.

One particularly noteworthy feature is that the 17.9 μm FIR transition is very strong, with large collision strengths and resonances just above the excitation threshold at $E \approx 0.1$ Ry. That yields a maximum effective collision strength $\Upsilon(T_e) > 2.0$ between 10^3 and 10^4 K; by comparison the strong 157 micron transition in C II has a value of ~ 1.6 (Blum & Pradhan 1991). Consequently, the excitation rate coefficient and emissivity (equations 3 and 4) would indicate strong observable intensity relative to other FIR lines from other elements (viz. Pottasch and Bernard-Salas). In addition, the energy dependence of $\Omega(E)$ in Fig. 3(a) leads to variation of more than a factor of 3 in $\Upsilon(T_e)$ in Fig. 3(b). Therefore, the intensity of the line is a sensitive indicator of temperature in the typical nebular range of 10^2–10^5 K, encompassing spectral formation in important sources such as PNe and SNRs.
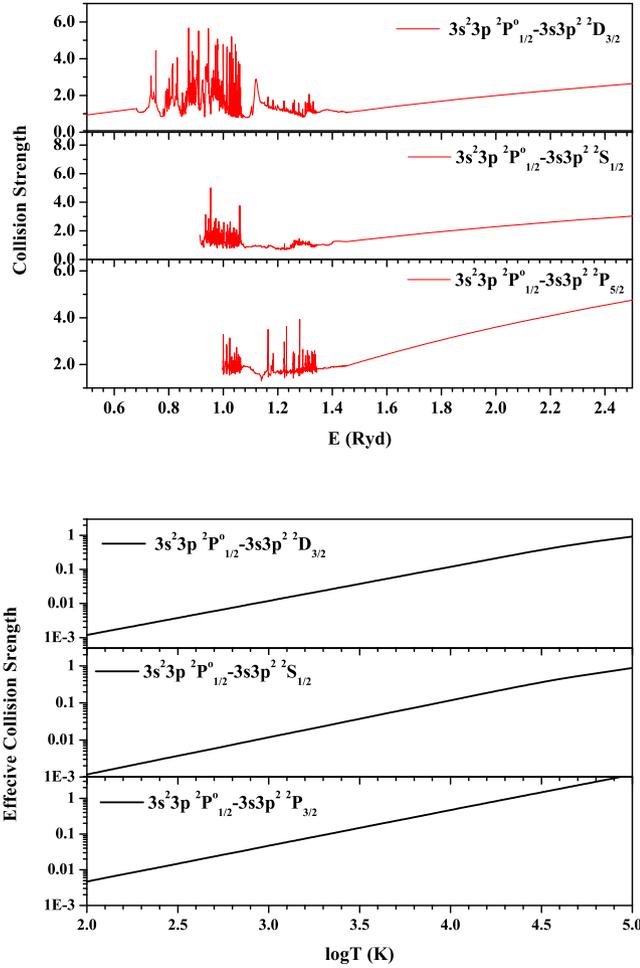
Figure 3. (a) Collision strengths $\Omega(E)$ for sample UV fine structure transitions from the ground level $^2P^o_{1/2} \rightarrow {}^2D_{3/2}, {}^2S_{1/2}, {}^2P_{3/2}$. For $E > 1.5$ Ry the Coulomb–Bethe form $\Omega(E) \sim \ln E$ is employed, typical of dipole allowed transitions at high energies and partial waves. (b) Maxwellian averaged effective collision strengths $\Upsilon(T_e)$ for the transitions in (a).

4.2 Allowed UV transitions

There are a number of intercombination and dipole allowed E1 transitions between the odd parity ground-state fine structure levels $3s^23p(^2P^o_{1/2-3/2})$ and the even parity $3s3p^2(^4P_{1/2, 3/2, 5/2}, {}^2D_{3/2, 5/2}, {}^2S_{1/2}, {}^2P_{1/2, 3/2})$ levels. However, laboratory and theoretical radiative data for measured wavelengths and Einstein A-values available from the National Institute of Standards and Technology show only the three transitions in the $^2P^o_{1/2,3/2}-{}^2D_{3/2,5/2}$. Fig. 3(a) presents sample collision strengths for fine structure components of dipole transitions in the three allowed multiplets. The BPRM calculations again show resonance structures below the highest target ion threshold at 1.45 Ry due to low-ℓ partial waves included in the calculations with $\ell_o \approx 10$. As these are E1 transitions, the collision strengths rise with increasing energy owing to divergent higher partial wave contributions $\ell > \ell_o$. The general form in the high-energy region may be approximated by the Bethe formula $\Omega \sim a \ln E$, where a is related to the dipole oscillator strength, assuming high-ℓ collisions as radiatively induced (Pradhan & Nahar 2011). We therefore match the BPRM collision strengths at 1.45 Ry to the Bethe expression. While there may be some uncertainty in the vicinity of this energy region, the overall behaviour of the collision strengths in

Fig. 3(a) appears to be correct [cf. Blum & Pradhan (1991) for C II collision strengths for similar transitions]. The effective collision strengths $\Upsilon(T_e)$ in Fig. 3(b) show the expected rising behaviour with temperature, typical of allowed transitions.

4.3 Maxwellian averaged collision strengths

In Table 1 we present the effective collision strengths (equation 3) for the four FIR and UV transitions reported herein. The tabulation is carried out at a range of temperatures typical of nebular environments 10^2-10^5 K. It is striking how much stronger the forbidden FIR 17.9 μm is relative to the allowed UV transitions, and dominates collisional excitation to all other levels by up to two orders of magnitude for temperatures between 100 and 10 000 K, although the values become comparable towards higher temperatures as shown in Fig. 3(b). That further numerically supports the approximation that the FIR line intensity may be little affected by excitation to higher levels.

4.4 Discussion

The results reported herein should enable spectral diagnostics of both the [P III] forbidden 17.9 μm line as well as UV transitions with a practically complete 18-level collisional-radiative atomic model. The FIR and UV lines cannot be observed with the same spectrometer and their spectral formation may be governed by different physical conditions, as well as subject to extinction that is highly wavelength dependent and would differentially attenuate line intensities. Some temperature dependence may be deduced from the energy behaviour inherent in the collision strengths data presented, and derived line emissivities. Based on extensive benchmarking of R-matrix data with experiments, we estimate the accuracy of the effective collision strengths between 10 and 20 per cent.

We may calculate nebular phosphorus abundance as outlined in Section 2 equations (1)–(5), based on the [P III] 17.9 μm line intensity ratio relative to H β. We assume a temperature 10^4 K, density 10^4 cm^{-3}, transition energy $h\nu = 0.069$ eV, solar P-abundance, and ionic ratio P III/P = 0.33. Using $\Upsilon(10^4$ K) from Table 1, the rate coefficient $q = 7.77 \times 10^{-8}$ cm^3 s^{-1} and $(4\pi/N_pN_e)\epsilon(17.9\,\mu m) = 7.33 \times 10^{-28}$ ergs cm^{-3} s^{-1}. Nebular recombination Hβ line intensities $(4\pi/N_pN_e)j(H\,\beta)$ are: 8.3×10^{-26} (Case A) and 1.24×10^{-25} ergs cm^3 s^{-1} (Case B). Therefore, $\epsilon(17.9\,\mu m)/H\,\beta = 8.8 \times 10^{-3}$ (Case A) and 5.9×10^{-3} (Case B), respectively. These $\epsilon(17.9\,\mu m)/H\,\beta$ line ratios lie in the range observed in several PNe, but the P-abundances heretofore derived are a factor of 3–4 lower than solar (viz. Pottasch & Bernard-Salas 2008); present work may yield higher abundances.

Further refinements can be made by considering additional atomic processes such as level-specific (e + P IV) → P III recombination-cascades, and fluorescent excitation from an external radiation field such as in PNe central stars with $T_{rad} \approx$ 80 000–120 000 K. A more elaborate calculation can be done using equation (2) that would combine the collisional-radiative model with a photoionization model that describes P-ionization states more accurately than, say, the P III/P value of 0.33 assumed above. However, these improvement would require extensive new atomic calculations for photoionization and (e + ion) recombination (e.g. Nahar et al. 2017). An interesting possibility is that of laser action in the 17.9 μm line, similar to that explored for the C II 157 micron transition (Peng & Pradhan 1994). Population inversion may occur owing to the extremely small magnetic dipole (M1) radiative decay rate A($^2P^o_{3/2}-{}^2P^o_{1/2}$) = 1.57×10^{-3} s^{-1} (NIST *Atomic Spectral Database*:

Table 1. Effective Maxwellian averaged collision strengths for FIR and UV transitions in P III.

Log$T$ (K) J–J' λ	$^2P^o$ 1/2–3/2 17.9 μm	$^2P^o$–^2D 1/2–3/2 1334.8 Å	$^2P^o$–^2S 1/2–1/2 998.6 Å	$^2P^o$–^2P 1/2–3/2 914.5 Å	Log$T$ (K) J–J' λ	$^2P^o$ 1/2–3/2 17.9 μm	$^2P^o$–^2D 1/2–3/2 1334.8 Å	$^2P^o$–^2S 1/2–1/2 998.6 Å	$^2P^o$–^2P 1/2–3/2 914.5 Å
2.0	7.73(−1)	1.20(−3)	1.18(−3)	1.13(−3)	3.6	2.19	4.76(−2)	4.68(−2)	4.51(−2)
2.1	9.45(−1)	1.50(−3)	1.48(−3)	1.43(−3)	3.7	2.16	5.99(−2)	5.89(−2)	5.67(−2)
2.2	1.13	1.90(−3)	1.86(−3)	1.79(−3)	3.8	2.10	7.54(−2)	7.41(−2)	7.14(−2)
2.3	1.33	2.39(−3)	2.34(−3)	2.26(−3)	3.9	2.04	9.50(−2)	9.33(−2)	8.99(−2)
2.4	1.52	3.00(−3)	2.95(−3)	2.84(−3)	4.0	1.97	1.20(−1)	1.18(−1)	1.13(−1)
2.5	1.70	3.78(−3)	3.72(−3)	3.58(−3)	4.1	1.90	1.51(−1)	1.48(−1)	1.43(−1)
2.6	1.85	4.76(−3)	4.68(−3)	4.51(−3)	4.2	1.83	1.90(−1)	1.86(−1)	1.79(−1)
2.7	1.98	5.99(−3)	5.89(−3)	5.67(−3)	4.3	1.77	2.39(−1)	2.34(−1)	2.26(−1)
2.8	2.08	7.54(−3)	7.41(−3)	7.14(−3)	4.4	1.73	3.00(−1)	2.93(−1)	2.84(−1)
2.9	2.16	9.50(−3)	9.33(−3)	8.99(−3)	4.5	1.69	3.75(−1)	3.63(−1)	3.56(−1)
3.0	2.20	1.20(−2)	1.18(−2)	1.13(−2)	4.6	1.65	4.63(−1)	4.43(−1)	4.45(−1)
3.1	2.23	1.51(−2)	1.48(−2)	1.43(−2)	4.7	1.60	5.62(−1)	5.32(−1)	5.55(−1)
3.2	2.24	1.90(−2)	1.86(−2)	1.79(−2)	4.8	1.55	6.70(−1)	6.32(−1)	6.91(−1)
3.3	2.25	2.39(−2)	2.34(−2)	2.26(−2)	4.9	1.47	7.87(−1)	7.45(−1)	8.64(−1)
3.4	2.24	3.00(−2)	2.95(−2)	2.84(−2)	5.0	1.39	9.19(−1)	8.82(−1)	1.09
3.5	2.22	3.78(−2)	3.72(−2)	3.58(−2)					

www.nist.gov). Equating $N_e q = A$, we obtain $N_e = 2.0 \times 10^4$ cm^{-3}. Therefore, at electron densities $N_e > 10^4$ cm^{-3}, electron impact excitation exceeds spontaneous decay, and population inversion and laser emission may occur in higher density SNRs or other sources.

4.5 Conclusion

Accurate collision strengths including fine structure with relativistic effects are computed for diagnostics of the [P III] forbidden FIR and allowed UV lines to enable a more precise re-examination of phosphorus abundance. The results show significant temperature dependence that should provide additional information on the physical environment and spectral formation. In particular, this work suggests searches for the [P III] FIR line using *Spitzer* IRS data and abundance determination. Further work is in progress on photoionization and collisional excitation of P-ions relevant to this investigation. All data are available from the authors and archived in S. N. Nahar's data base NORAD at: www.astronomy.ohio-state.edu~nahar, and TIPTOPBase at the Opacity Project/Iron Project webpage: http://cdsweb.u-strasbg.fr/OP.htx.

REFERENCES

Asplund M., Grevesse N., Jacques Sauval A., Scott P., 2009, ARA&A, 209, 47

Blum R. D., Pradhan A. K., 1991, Phys. Rev. A, 44, 6123

Burke P. G., 2011, R-Matrix Theory of Atomic Collisions., Springer Series on Atomic, Optical, and Plasma Physics Series on Atomic, Optical, and Plasma Physics

Eissner W., Jones M., Nussbaumer H., , 1974, Comput. Phys. Commun., 8:270

Ganas P. S., 1998, Eur. Phys. J. D, 1, 165

Koo B-C., Lee Y-H., Moon D-S., Yoon S-C., Raymond J.C., 2013, Science, 342:1346

Maas Z. G., Pilachowski C. A., Cescutti G., 2017, ApJ, 841, 108

Nahar S. N. et al., 2017a, New Astronomy, 50, 19

Nahar S. N., 2017b, MNRAS, 469, 3225

Nahar S. N et al. et al. , 2017, J. Quant. Spectrosc. Radiat. Transfer, 187, 215

Otsuka M., Mexner M., Riebel D., Hyung S., Tajitsu A., Izumiura H., 2011, ApJ, 729, 39

Peng J., Pradhan A. K., 1994, ApJ, 432, L123

Pottasch S. R., Beintema D. A., 1999, A&A, 347, 975

Pottasch S. R., Bernard-Salas J., 2008, A&A, 490, 715

Pottasch S. R., Bernard-Salas J., Roelig T. L., 2008, A&A, 481, 393

Pradhan A. K., Nahar S. N., 2011, Atomic Astrophysics and Spectroscopy. Cambridge Univ. Press, Cambridge

Wang H., Jiang G., Duan J., 2016, Eur. Phys. J. D, 70, 122

This paper has been typeset from a TEX/LATEX file prepared by the author.